JOURNAL OF APPLIED PHYSICS **118**, 045713 (2015)

Electron-phonon interaction and scattering in Si and Ge: Implications for phonon engineering

Nandan Tandon,[1,2,a)] J. D. Albrecht,[1,b)] and L. R. Ram-Mohan[3,c)]
[1]*Department of Electrical and Computer Engineering, Michigan State University, East Lansing, Michigan 48824, USA*
[2]*Department of Physics, Worcester Polytechnic Institute, Worcester, Massachusetts 01609, USA*
[3]*Departments of Physics and Electrical and Computer Engineering, Worcester Polytechnic Institute, Worcester, Massachusetts 01609, USA*

(Received 29 April 2015; accepted 17 July 2015; published online 29 July 2015)

We report *ab-initio* results for electron-phonon (e-ph) coupling and display the existence of a large variation in the coupling parameter as a function of electron and phonon dispersion. This variation is observed for all phonon modes in Si and Ge, and we show this for representative cases where the initial electron states are at the band gap edges. Using these e-ph matrix elements, which include all possible phonon modes and electron bands within a relevant energy range, we evaluate the imaginary part of the electron self-energy in order to obtain the associated scattering rates. The temperature dependence is seen through calculations of the scattering rates at 0 K and 300 K. The results provide a basis for understanding the impacts of phonon scattering vs. orientation and geometry in the design of devices, and in analysis of transport phenomena. This provides an additional tool for engineering the transfer of energy from carriers to the lattice. © *2015 AIP Publishing LLC*.
[http://dx.doi.org/10.1063/1.4927530]

I. INTRODUCTION

Calculations of the electron-phonon (e-ph) interaction have typically relied on parameterized empirical models to dramatically reduce the computational cost and complexity. There are many examples in the literature. The rigid pseudo-ion model has been used to calculate the phonon-mediated Γ-Δ transitions in Si for the longitudinal optic (LO), the transverse optic (TO), the longitudinal acoustic (LA), and transverse acoustic (TA) mediated transitions.[1] The e-ph coupling constants for the group IV elements have been calculated in the approximation of the metallic β-Sn structure.[2] Also, a Harris functional approach has been used to investigate the e-ph interaction in Si within the rigid ion approximation and better deformation potentials compared to previous models, and the prediction of high dispersion in the e-ph interaction was reported.[3] The latter method does not evaluate the ground state charge density self-consistently but rather assumes that the charge density is the superposition of atomic charge densities.

In other work, the e-ph matrix elements and deformation potentials in Si and Ge were calculated in the quasi-ion model.[4] Specifically, e-ph matrix elements for indirect optical absorption, inter-valley matrix elements, and intra-valley deformation potentials were calculated only for $\mathbf{k} = 0$ states. Matrix elements of $\partial V(\mathbf{r})/\partial \mathbf{R}_a^m$ were obtained describing the change in the crystal potential $V(\mathbf{r})$ due to a unit displacement of an ion of type a in cell m. The TA phonon dispersion curves in this model do not flatten out to correspond to the experimentally observed behavior at the L- and X-points. The calculation is essentially for the fixed momentum transfers in the $\Gamma \rightarrow X$ transitions and $X \leftrightarrow X$ inter-valley transitions in Si, as well as the $\Gamma \rightarrow L$ and $L \leftrightarrow L$ matrix elements in Ge. Finally, first principles approaches have recently been used to evaluate mobility in Si and Ge using pseudopotential or the tight-binding approaches.[5–8]

We have recently shown that e-ph coupling varies significantly throughout the Brillouin zone (BZ) in diamond.[9] In this article, we explore whether similar behavior is observed in the technologically important semiconductors Si and Ge. Earlier, transport calculations have been performed within the long-wavelength approximation or by considering an isotropic coupling constant for different phonon modes.[10,11] These approximations can be avoided with modern computational resources and the availability of parameter-free *ab-initio* techniques that allow the study of this variation in detail. For example, a first-principles study of the variation in lattice thermal conductivity with carrier concentration of Si considering both the phonon-phonon and e-ph interactions has predicted a reduction of about 45% in the thermal conductivity due to the e-ph interaction, which is a substantial correction.[12] A recent study on hot electrons in GaAs has shown that all optical and acoustic phonons contribute substantially to electron-phonon scattering, contrary to earlier understanding.[13]

Here, we show that e-ph matrix elements for all six phonon branches in Si and Ge have characteristic dispersions. Several cases are presented to highlight the effect. Calculations are performed both for electrons at the valence band maximum (VBM) and at the local conduction band minima (CBM). The e-ph coupling for the three acoustic and the three optical phonon branches is displayed along the edge of the irreducible BZ. We complete the study by evaluating the e-ph coupling on a very dense BZ grid to compute the scattering rates using the imaginary part of electron

a)Electronic mail: tandonna@msu.edu
b)Electronic mail: jalbrech@msu.edu
c)Electronic mail: lrram@wpi.edu

self-energy. The results are shown in Sec. III and compared with earlier work in detail. This is followed by concluding remarks in Sec. IV. The direction dependence of the coupling could be exploited in order to engineer the energy relaxation of hot carriers in device channels by orienting them crystallographically. By dictating the dominant crystal momentum components, it should be possible to alter the energy relaxation to either favor or suppress transfer of energy to the lattice.

II. METHODOLOGY

The work reported here was performed using QUANTUM ESPRESSO[14] with norm-conserving pseudopotentials within the local density approximation[15] for the exchange-correlation potential. Lattice dynamics were computed using density functional perturbation theory.[16] The published electron-phonon Wannier (EPW) framework[17] is used to evaluate the e-ph matrix elements, electron self-energy, and the scattering rate for phonon emission by determining the electron self-energy function. We carry out our calculations on unit cells of Si and Ge with optimized lattice parameter 10.21 a.u. and 10.61 a.u. (experimental lattice parameters are 10.26 a.u. and 10.69 a.u., respectively). A kinetic energy cutoff of 65 Ry is used for the plane-wave basis, and the BZ sampling is on $8 \times 8 \times 8$ Monkhorst-Pack k-point grids.[18] Our calculations result in an indirect bandgap of $\sim$0.54 eV for Si and $\sim$0.48 eV for Ge (both low given the local density approximation).

Density functional perturbation theory[16] is used to evaluate the phonon dispersion and associated deformation potentials over an $8 \times 8 \times 8$ q-point grid for the phonons and a basis of 12 maximally localized Wannier functions to describe the valence band and the lowest conduction band.[19]

The e-ph matrix elements $g^{\nu}_{mn}(\mathbf{k},\mathbf{q})$ are defined as

$$g^{\nu}_{mn}(\mathbf{k},\mathbf{q}) = \langle \psi_{m,\mathbf{k}+\mathbf{q}} | \partial_{\mathbf{q}\nu} V | \psi_{n,\mathbf{k}} \rangle, \tag{1}$$

where m and n are initial and final electron band indices with wavevectors $\mathbf{k}$ and $\mathbf{k}+\mathbf{q}$, respectively, and $\partial_{\mathbf{q},\nu}$ is the derivative of the self-consistent potential associated with a phonon of wavevector $\mathbf{q}$ in branch ν. The matrix element has been evaluated over a grid of $50 \times 50 \times 50$ $\mathbf{q}$ points to evaluate the imaginary part of the self-energy ($\mathcal{I}m(\Sigma^{e-ph}_{n\mathbf{k}})$) within EPW. The real and imaginary parts of the electron self-energy ($\Sigma^{e-ph}_{n\mathbf{k}}$) are given by

$$\Sigma^{e-ph}_{n\mathbf{k}} = \sum_{\mathbf{q},\nu,m} W_{\mathbf{q}} |g^{\nu}_{mn}(\mathbf{k},\mathbf{q})|^2 \left[\frac{n(\omega_{\mathbf{q},\nu}) + f(\epsilon_{m,\mathbf{k}+\mathbf{q}})}{\epsilon_{n,\mathbf{k}} - \epsilon_{m,\mathbf{k}+\mathbf{q}} + \omega_{\mathbf{q},\nu} - i\eta} + \frac{n(\omega_{\mathbf{q},\nu}) + 1 - f(\epsilon_{m,\mathbf{k}+\mathbf{q}})}{\epsilon_{n,\mathbf{k}} - \epsilon_{m,\mathbf{k}+\mathbf{q}} - \omega_{\mathbf{q},\nu} - i\eta} \right], \tag{2}$$

where $W_{\mathbf{q}}$ are the BZ weights associated with each $\mathbf{q}$, f is the Fermi occupancy function, $\epsilon_{n,\mathbf{k}}$ is the electron energy in band n and state $\mathbf{k}$, $\hbar\omega_{\mathbf{q},\nu}$ is the phonon energy in band ν and state $\mathbf{q}$, and n is the Bose occupation factor. In our numerical calculation, the energy-conserving δ-function is approximated by a Gaussian of width 0.001 eV. The e-ph scattering rates associated with e-ph interactions are given by $(\tau^{e-ph}_{n\mathbf{k}})^{-1} = 2[\mathcal{I}m(\Sigma^{e-ph}_{n\mathbf{k}})]/\hbar$. For further details, the reader is referred to Ref. 9.

We consider three cases of the initial electron momentum and display the variation in the e-ph coupling. For two cases, the initial electron is at Γ ($\mathbf{k}=0$) and $\mathbf{q}$ is allowed to vary such that the momentum of the scattered electron ($\mathbf{k}'$) is given by $\mathbf{k}' = \mathbf{q}$. For the third case, the initial electron state is at the absolute CBM at the Δ symmetry point for Si and at the L-point for Ge and hence $\mathbf{k}' \neq \mathbf{q}$.

III. RESULTS

A. Electron-phonon coupling

1. Silicon

The e-ph coupling in Si between an initial electron at the VBM and the lowest three phonon modes is shown in Fig. 1(a) (Si,VBM). The e-ph coupling to the TA mode is much smaller compared with coupling to the LA mode, and this is expected to be the case because the TA mode only involves shear strain, whereas the LA mode results in shear strain and volume dilation.[20] The e-ph matrix elements for the TA modes are zero at the special points Γ, L, and X, and the magnitudes of the matrix elements are much lower compared to the LA mode elsewhere in the BZ. Figure 1(b) (Si,VBM) shows the e-ph coupling for the same initial electron state with the optical phonons. The e-ph coupling is much higher for the optical modes as compared with the acoustic phonon modes and the variation is $\sim$150 meV. Figures 1(a) (Si,CBM/Γ) and 1(b) (Si,CBM/Γ) show the e-ph coupling between an initial electron at the local CBM at Γ and the acoustic and optical phonon modes, respectively. The emitted electron momentum corresponds to the lowest conduction band. The e-ph coupling between an initial electron at the CBM at Δ and phonon modes is shown in Fig. 1(a) (Si,CBM/Δ) for the acoustic modes and in Fig. 1(b) (Si,CBM/Δ) for the optical modes. As seen in Ref. 9 for diamond, the coupling to the optical modes vanishes in the long wavelength limit, which is consistent with the same symmetry arguments.

2. Germanium

The e-ph couplings of the acoustic and optical phonons modes are also shown in Fig. 1. The dramatic high or low magnitudes of e-ph coupling at special points in the BZ are attributed to the crossings of phonon bands and also to the change in direction of the q-vector along the edge of irreducible BZ. The phonon dispersions in Si and Ge are almost identical except for the lower magnitude of the phonon

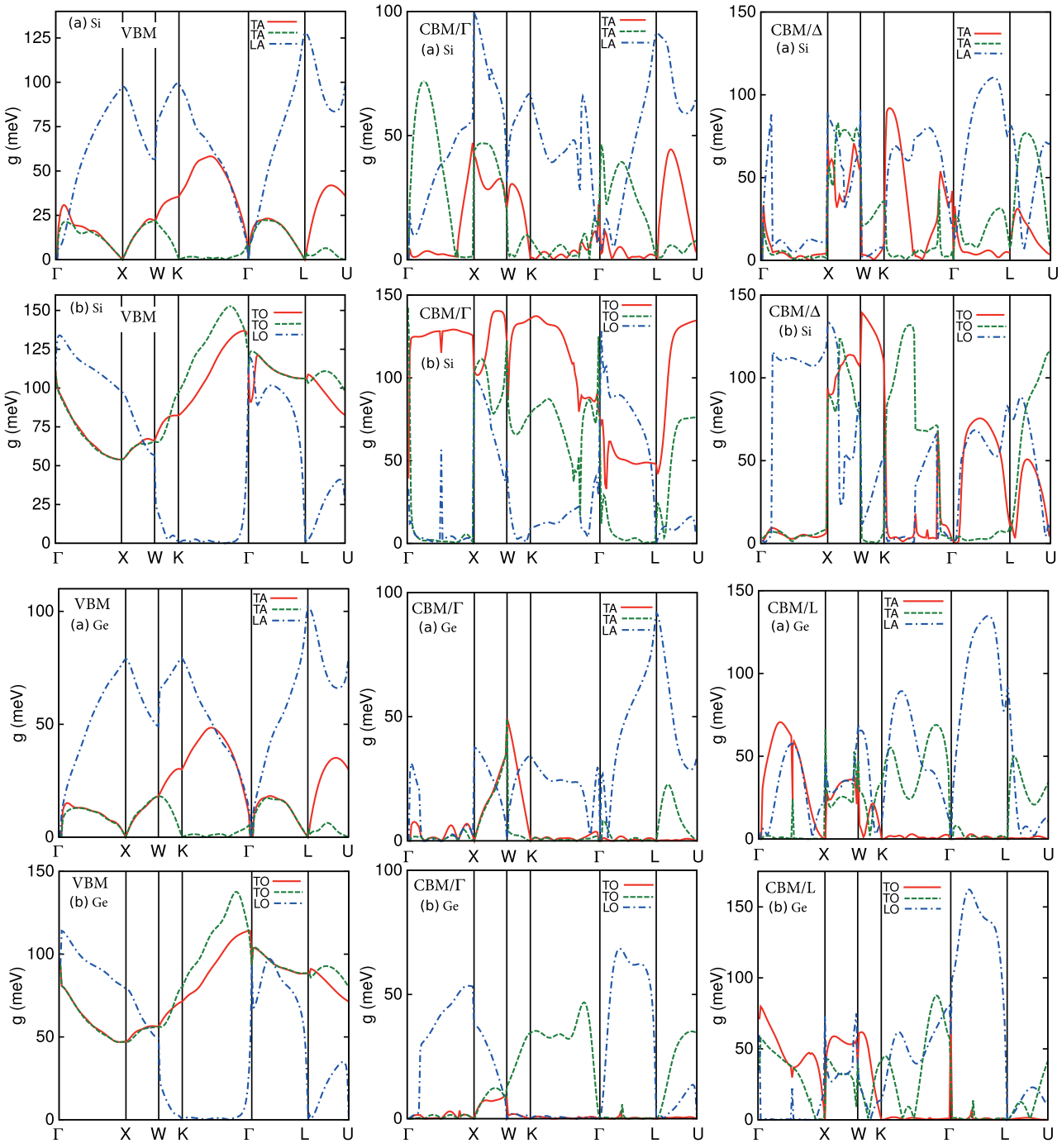

FIG. 1. The variation of the e-ph coupling in Si and Ge is shown. The initial electron state either is the VBM, the absolute CBM (labeled CBM/Δ for Si and CMB/*L* for Ge), or the local CBM at the zone center (labeled CMB/Γ). The e-ph coupling for each phonon mode is displayed for the labeled initial electron energy for (a) acoustic phonon branches TA (continuous and dashed) and LA (dashed-dotted); and (b) the optical phonon branches TO (continuous and dashed) and LO (dashed-dotted).

frequencies in Ge. Figures 1(a) (Ge,CBM/Γ) and 1(b) (Ge,CBM/Γ) show the e-ph coupling between an initial electron at the local CBM at Γ and the acoustic and optical phonons, respectively. Again, the emitted electron momentum corresponds to the lowest conduction band. The case of the initial electron at the CBM in Ge and its couplings with the phonon modes are shown in Fig. 1(a) (Ge,CBM/*L*) for the acoustic phonon modes and in Fig. 1(b) (Ge,CBM/*L*) for the optical modes. Since the CBM for Ge and Si is at different symmetry points, the nature of the e-ph coupling is expected to be different and this is evident from the plots. One significant difference between the two cases is that for Si, the matrix element for the optical modes was negligible for long wavelength limit, whereas for Ge it is non-zero, but is zero at *L*.

B. Electron linewidth and scattering rate

1. Silicon

Figures 2(a) and 2(b) show the imaginary part of the e-ph self-energy at 0 K and 300 K. This figure shows the **k**

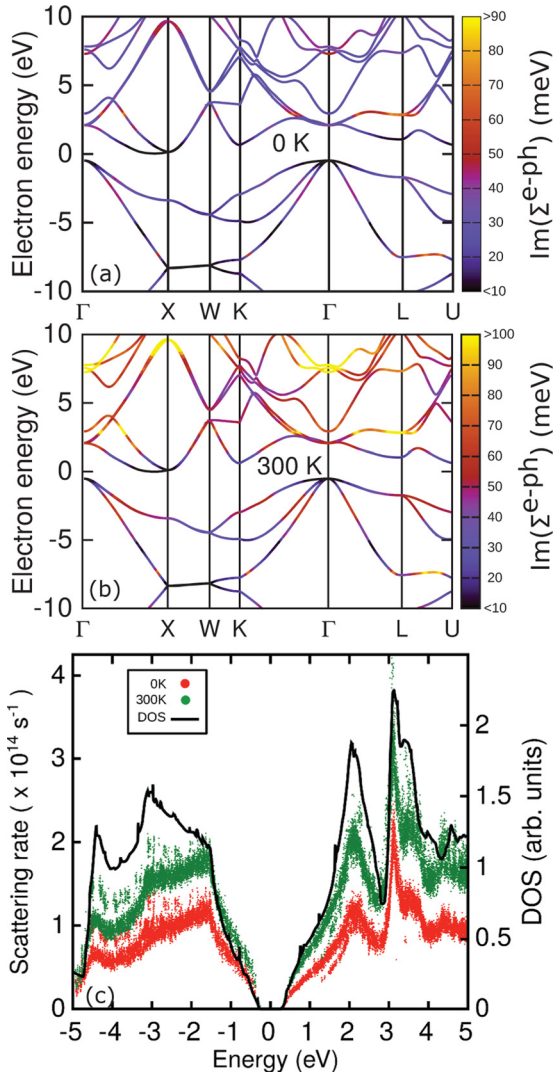

FIG. 2. The band structure of Si with a color map of the $\mathcal{I}m(\Sigma^{e-ph}_{n\mathbf{k}})$ at (a) 0 K and (b) 300 K with zero of energy axis placed at the CBM. The scattering rate associated with the e-ph self-energy at 0 K and 300 K and the electronic DOS are shown in (c), with zero of energy placed at the midpoint of the band gap.

dependence of the $\mathcal{I}m(\Sigma^{e-ph}_{n\mathbf{k}})$ for different electron energies. We see that the self-energy, as expected, is larger for higher temperature. At the VBM and CBM, the self-energy is negligible (<10 meV) due to the absence of states in the bandgap region. For 0 K, the local conduction band minima also have a very low magnitude, but on increasing the temperature to 300 K, these minima will contribute to the scattering. At both temperatures, it is clearly seen that for initial electron energy corresponding to the second lowest conduction band at L, the e-ph self-energy is high and one can expect higher e-ph scattering rates corresponding to these energies. In addition, one can draw inferences about the scattering rates or inversely the hot carrier relaxation times. Near the band edges, the relaxation times are high, whereas few hundred millielectron volts away from the band edges, the relaxation times are much shorter. High scattering rates are observed for [111] direction at low energies in the conduction band.

Figure 2(c) shows the e-ph scattering rates for Si and their variation with initial electron energy for a grid of $20 \times 20 \times 20$ **k**-points. The electronic density of states (DOS) of Si shows the phase space available for scattering. The origin of the energy axis corresponds to the CBM. This displays that the scattering rate is proportional to the available electron states and is proportional to the density of states. The overall shape and magnitude of the scattering rate compares well with other earlier reports.[7,21] We also observe that 1 eV above the CBM a feature of lower scattering rates due to the presence of *L* valley.

2. Germanium

The electron linewidths for Ge at 0 K are shown in Fig. 3(a) as a color map over the band structure of Ge. The $\mathcal{I}m(\Sigma^{e-ph}_{n\mathbf{k}})$ has negligible magnitude around the top of the valence band and the conduction band valleys at *X*, Γ, and *L*. This behavior around the band gap is expected because there is a negligible region in the phase-space available in this region where an emitted electron can be accommodated. Similarly, Fig. 3(b) shows the color map of imaginary part of

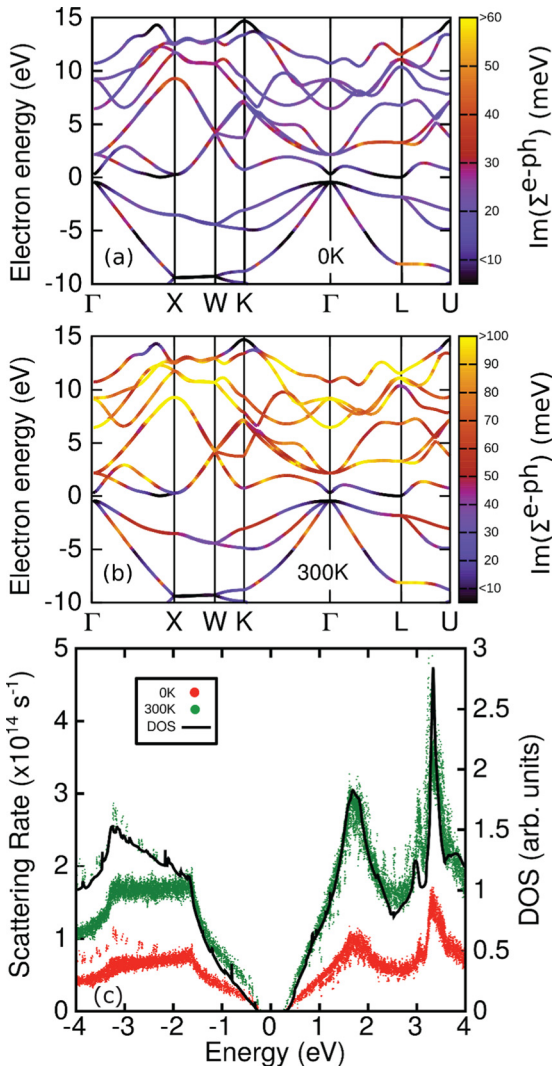

FIG. 3. The band structure of Ge with a color map of the $\mathcal{I}m(\Sigma^{e-ph}_{n\mathbf{k}})$ at (a) 0 K and (b) 300 K with zero of energy axis placed at the CBM. The scattering rate associated with the e-ph self-energy at 0 K and 300 K and the electronic DOS are shown in (c), with zero of energy placed at the midpoint of the band gap.

the self-energy in Ge at 300 K. Here as well, it is seen that the self-energy has negligible magnitude at the band edges. In addition, it can be seen that since the self-energy along $\Gamma \rightarrow L$ is relatively low, the e-ph scattering rate along this direction would be low. The scattering rate for the initial electron at Γ is low. Tyuterev *et al.*[6] have observed that the deformation potential for the virtual transitions in which the initial electron state is Γ and final states are at the L, Δ, or X valley minima is zero for all of the transverse phonon modes. This would result in a lowered scattering rate, as expected from the self-energy in Fig. 3(b). Electron-phonon scattering rates are shown in Fig. 3(c) for 0 K and 300 K as a function of energy for the electron in Ge along with the electron DOS. The origin of the energy axis corresponds to the middle of the bandgap. The trend of the scattering rates shown here compares well with the recent work[7] and references therein. The strong dependence of the scattering rates on the electronic DOS is seen in Fig. 3(c).

IV. CONCLUDING REMARKS

In this article, we presented *ab initio* calculations of the e-ph coupling in Si and Ge. We demonstrated that there exists a large variation in the magnitude of the e-ph coupling along different crystallographic directions by evaluating the matrix element over the typical edge of the IBZ in these materials. This variation is shown to exist in all the phonon branches. This observation emphasizes the need to go beyond the long-wavelength approximation typically employed in such analysis.

Phonon engineering concepts in semiconductor devices and nanostructures can use these orientation-dependent scattering rates as a basis for tailoring transport phenomena or analysis by Monte Carlo methods. Ultimately, the ability to tune the energy transfer to the lattice by device geometry, such as channel orientation, would enable thermal management concepts local to the junction of the electronic device. These phonon engineering concepts would, of course, have to take into account the presence of surfaces or interfaces specific to a given device. However, the results presented here could be used within material regions larger than the mean free path of the phonons.

We also evaluated the e-ph matrix elements on a fine grid to compute the associated scattering rates in these materials. The scattering rate was calculated by taking the imaginary part of the electron self-energy within EPW. The character of the scattering rate was shown first for the case where electron energy is varied as in the band structure for the material. Such a picture displays the variation in scattering along crystallographic directions, which is relevant for device design to choose appropriate directions of interest for lower scattering. In addition to this, we also computed the scattering rate for a dense grid, which shows the variation as a function of the energy of the electron. This allows us to observe that the scattering rate has lower value in Si when the phase-space around the L valley is limited. Since Ge has three CB valleys within a small energy window, such a region of lower scattering rate at high energies is not prominent and the scattering rate monotonically increases with energy. As expected, the results are consistent in that for higher temperatures, the scattering rates are much higher because the phonon occupation is higher and the electron distribution is spread out in energy allowing more available scattering states.

ACKNOWLEDGMENTS

We thank F. Giustino for discussions on the use of the EPW computer program and physical issues connected with it. The work at WPI has been supported by AFRL (FA8650-10-1-7046) and ONR (N00014-13-1-0021). The work at MSU was supported by DARPA (N66001-14-1-4038).

[1]O. J. Glembocki and F. H. Pollak, Phys. Rev. Lett. **48**, 413 (1982).
[2]K. J. Chang and M. L. Cohen, Phys. Rev. B **34**, 4552 (1986).
[3]P. D. Yoder, V. D. Natoli, and R. M. Martin, J. Appl. Phys. **73**, 4378 (1993).
[4]M. Klenner, C. Falter, and W. Ludwig, Ann. Phys. **504**, 24 (1992).
[5]O. D. Restrepo, K. Varga, and S. T. Pantelides, Appl. Phys. Lett. **94**, 212103 (2009).
[6]V. G. Tyuterev, S. V. Obukhov, N. Vast, and J. Sjakste, Phys. Rev. B **84**, 035201 (2011).
[7]D. Rideau, W. Zhang, Y. M. Niquet, C. Delerue, C. Tavernier, and H. Jaouen, in *Proceedings of International Conference on Simulation of Semiconductor Processes and Devices (SISPAD)* (2011), pp. 47–50.
[8]Y. M. Niquet, D. Rideau, C. Tavernier, H. Jaouen, and X. Blase, Phys. Rev. B **79**, 245201 (2009).
[9]N. Tandon, J. D. Albrecht, and L. R. Ram-Mohan, Diamond Relat. Mater. **56**, 1 (2015).
[10]M. V. Fischetti and S. E. Laux, Phys. Rev. B **38**, 9721 (1988).
[11]M. V. Fischetti, Phys. Rev. B **44**, 5527 (1991).
[12]B. Liao, B. Qiu, J. Zhou, S. Huberman, K. Esfarjani, and G. Chen, Phys. Rev. Lett. **114**, 115901 (2015).
[13]M. Bernardi, D. V. Fowler, C. S. Ong, J. B. Neaton, and S. G. Louie, Proc. Natl. Acad. Sci. U. S. A. **112**, 5291 (2015).
[14]P. Giannozzi, S. Baroni, N. Bonini *et al.*, J. Phys.: Condens. Matter **21**, 395502 (2009).
[15]J. P. Perdew and A. Zunger, Phys. Rev. B **23**, 5048 (1981).
[16]S. Baroni, S. d. Gironcoli, A. D. Corso, and P. Giannozzi, Rev. Mod. Phys. **73**, 515 (2001).
[17]J. Noffsinger, F. Giustino, B. D. Malone, C. H. Park, S. G. Louie, and M. L. Cohen, Comput. Phys. Commun. **181**, 2140 (2010).
[18]H. J. Monkhorst and J. D. Pack, Phys. Rev. B **13**, 5188 (1976).
[19]A. A. Mostofi, J. R. Yates, Y.-S. Lee, I. Souza, D. Vanderbilt, and N. Marzari, Comput. Phys. Commun. **178**, 685 (2008).
[20]P. Y. Yu and M. Cardona, *Fundamentals of Semiconductors*, 4th ed. (Springer, Berlin, 2010).
[21]M. Bernardi, D. V. Fowler, J. Lischner, J. B. Neaton, and S. G. Louie, Phys. Rev. Lett. **112**, 257402 (2014).